Available online at www.sciencedirect.com
SCIENCE DIRECT®
Polymer 44 (2003) 6995–7005
polymer
www.elsevier.com/locate/polymer

Spherulite formation from microphase-separated lamellae in semi-crystalline diblock copolymer comprising polyethylene and atactic polypropylene blocks

Masaya Ueda[a], Kazuo Sakurai[b,*], Shigeru Okamoto[c], David J. Lohse[d], William J. MacKnight[e], Seiji Shinkai[f], Shinichi Sakurai[a*], Shunji Nomura[a]

[a]*Department of Polymer Science and Engineering, Kyoto Institute of Technology, Matsugasaki, Sakyo-ku, Kyoto 606-8585, Japan*
[b]*Department of Chemical Processes and Environments, The University of Kitakyushu, 1-1 Hibikino, Wakamatsu-ku, Fukuoka 808-0135, Japan*
[c]*Department of Material Science and Engineering, Nagoya Institute of Technology, Gokiso-cho, Showa-ku, Nagoya 466-8555, Japan*
[d]*ExxonMobil Research and Engineering Company, Annandale, NJ 08801-3059, USA*
[e]*Department of Polymer Science and Engineering, University of Massachusetts, Amherst, MA 0100-4530, USA*
[f]*Chemotransfiguration Project, Japan Science and Technology Cooperation, Kurume, Fukuoka 839-0861, Japan*

Received 17 January 2002; received in revised form 23 June 2003; accepted 15 July 2003

Abstract

The characteristics of crystallization in a semi-crystalline block copolymer have been experimentally examined using small-angle X-ray scattering and small-angle light scattering. For this purpose, a flow-oriented polyethylene-*block*-(atactic polypropylene) diblock copolymer with $M_w = 113$ kg/mol and a polyethylene volume fraction of 0.48 was used. First of all, the crystallization was found to be much suppressed as compared to that of polyethylene homopolymer (homo-PE), as evidenced by a crystallinity that was approximately one-third of homo-PE. Spherulite growth with rupturing the microphase-separated lamellae (micro-LAM) was found at crystallization temperatures in the range $95 \leq T_c \leq 101$ °C. That is, spherulites can grow even if the crystallization is initiated in the spatially confining micro-LAM structure. However, it was further found that the micro-LAM structure did not co-exist with a spherulite. On the other hand, at much lower crystallization temperatures ($T_c < 95$ °C), the micro-LAM structure was retained whereas no spherulites formed. The suppression of spherulite formation can be accounted for by an *auto-decelerating effect* of nuclei in a confining microdomain space.

Keywords: Spherulite formation; Diblock copolymer; Polyethylene

1. Introduction

Microdomain formation in a block copolymer comprising one or more crystallizable blocks results either from segregation due to immiscibility of the blocks [1] or by crystallization of the blocks [2]. Pioneering experimental work by Cohen et al. [3] and that by Seguela and Prud'homme [4] have demonstrated that the final morphology attained in a crystalline block copolymer depends on the thermal history of the samples. They showed that the microdomain structures obtained when microphase separation precedes crystallization could be quite different from that when crystallization occurs first. For the PE/PB system studied by Cohen et al. [3], crystallization occurred within pre-existing microphase-separated domains without rupturing the structure. On the other hand, Nojima et al. [5] showed an example where the microdomain morphology was ruptured by subsequent crystallization. In this case, the crystallization was carried out just below the microphase separation temperature, so that the energy barrier to rupture the pre-existing microdomain morphology is low and it can be overcome by the subsequent crystallization. Ryan and coworkers [6] further discussed a relationship between spherulite growth and the preservation of microdomain structures. They found that the pre-existing microphase-separated structure was ruptured due to chain folding, which finally grew into spherulites. However, the chain folding did

* Corresponding authors. Tel.: +81-93-695-3294; fax: +81-93-695-3368.
E-mail addresses: sakurai@env.kitakyu-u.ac.jp (K. Sakurai), shin@ipc.kit.ac.jp (S. Sakurai).

0032-3861/$ - see front matter © 2003 Elsevier Ltd. All rights reserved.
doi:10.1016/S0032-3861(03)00697-9

not always result in the rupture of the microphase-separated domains. As a matter of fact, numerous studies revealed preservation of the microdomain structures in which the crystallizable moiety can crystallize, and in turn, the microphase-separated lamellae (micro-LAM) and crystalline lamellae (cryst-LAM) co-exist [3,7,8]. Some of us have already reported the co-existence of micro-LAM and cryst-LAM for a polyethylene-*block*-poly(atactic propylene) diblock copolymer sample (DEP113) [9], which is also mainly used in the present study.

Whether or not the micro-LAM is preserved has so far been discussed in terms of the degree of segregation [5]. Nevertheless, we have found for our semi-crystalline DEP113 sample in the strong-segregation regime that the rupture of the pre-existing micro-LAM structures depends on the crystallization temperature (T_c). Interestingly, the rupture took place for a shallower quench ($95 \leq T_c \leq 97$ °C; the melting temperature, $T_m = 105$ °C) while it did not take place for a deeper quench ($T_c \leq 93$ °C). This finding requires a new type of interpretation. Furthermore, it is of great interest to examine whether spherulites can co-exist with micro-LAM structures. Namely, can a spherulite, which is initiated in a crystallizable microdomain structure, grow without rupturing the pre-existing micro-LAM structures and their regularity? Inaba et al. [10] studied a crystalline polymer blend having a co-continuous percolated domain structure in the melt and observed that spherulites much larger than the phase-separated structures were formed. It was speculated that crystalline fibrils can grow through a channel of a crystallizable domain to form a large spherulite. Terada et al. [11] have recently reported 'draining' spherulite growth (namely, growth without impingement) upon collision of the two growing spherulites consisting of different components in a binary blend of crystalline polymers. Although those studies for polymer blends differs in the size of phase-separated domains from the case of semi-crystalline block copolymers, it has been commonly suggested that three-dimensional continuity of phase-separated domains may be required for spherulite formation. Meanwhile, if the crystallizable domain lacks three-dimensional continuity, it is expected that the formation of the spherulite is hindered or much suppressed. Nevertheless, Register and coworkers [12] reported spherulite formation in this case. However, no direct confirmation of the co-existence of micro-LAM and spherulites is available from their results. Although an earlier work by Register and coworkers [2] and a work by Kofinas and Cohen [13] revealed a concurrent formation of micro-LAM and spherulites, this is rather ascribed to crystallization from a one-phase melt in the absence of pre-existing microphase-separated domains.

Despite its importance for controlling the final morphology, much is still unknown for the relationship between spherulites and micro-LAM structures. Especially, we were motivated to show direct experimental evidence of rupture of the pre-existing micro-LAM structures upon a spherulite formation even in strongly segregated semi-crystalline block copolymers. Since in the strong-segregation regime the degree of confinement of the micro-LAM is significant, it has been believed that if the micro-LAM are not continuous, there can be no formation of spherulites. For the purpose of this study, we utilized a diblock copolymer comprising polyethylene (PE) and atactic polypropylene (aPP) blocks, which is in the strong-segregation regime in the melt state. Since the formation of spherulites in the crystallizable domain without three-dimensional continuity is to be studied, it is required to prepare well-aligned micro-LAM with only two-dimensional continuity in the melt in prior to crystallization. Besides a single crystal of the micro-LAM with perfect alignment, through-path of crystalline microdomains is formed at a grain boundary [14] so that three-dimensional continuity of the crystalline microphase cannot be thoroughly ruled out. To obtain well-aligned micro-LAM, a planar extensional flow was imposed to the sample at an elevated temperature above T_m of PE according to the previously reported protocol [9,15]. Then, the spherulite formation was examined mainly by the depolarized small-angle light scattering technique (H_v-SALS) upon quenching the flow-oriented sample to several values of T_c.

2. Experimental

2.1. Block copolymer sample

A symmetric PE-*block*-aPP diblock copolymer (DEP113) was employed to study spherulite growth in the presence of micro-LAM structures. The DEP113 sample consisted of nearly equal volume fractions of crystallizable PE blocks and amorphous aPP blocks. For this constitution, the difference between the glass transition temperature of the aPP blocks and the melting temperature of the PE blocks is about 100 °C, which is large enough to isolate the crystallization free from influence of the glass transition. Other advantages of this sample are attributed to the fact that the PE crystal structure and its crystallization kinetics have been well studied [16].

The DEP113 sample was prepared through hydrogenation of poly(2-methyl-1,3-pentadiene)-*block*-polybutadiene [17]. The weight-average molecular weight (M_w) was 113 kg/mol, the heterogeneity index for the molecular weight distribution (M_w/M_n) was 1.1, where M_n denotes the number-average molecular weight, and the volume fraction of the PE blocks in the melt state was 0.48. The content of the ethyl branch was 3.0 mol% for the PE blocks. A differential scanning calorimetry (DSC) revealed that T_m of the PE moiety was 105 °C on heating at 10 °C/min. Thus, the crystallization temperatures examined in the present study (93–101 °C) were well below T_m (≈105 °C).

2.2. Small-angle X-ray scattering

The microphase-separated structures were analyzed by the one-dimensional small-angle X-ray scattering (1D-SAXS) technique at the BL-15A SAXS beamline (PF, Tsukuba, Japan) [18,19]. The X-ray beam was focused by a bent Ge(111) monochromator and a bent quartz mirror coated with platinum. The wavelength (λ) was tuned to 0.150 nm. More details of the BL-15A beamline are described elsewhere [18,19]. The position-sensitive proportional counter was utilized for static and time-resolved measurements.

To check the orientation of the micro-LAM structures, the two-dimensional SAXS (2D-SAXS) technique was employed. The measurements were performed at the RIKEN structural biology beamline I (BL45XU) at the SPring-8, Hyogo, Japan. It is an undulator beamline, providing a high flux of X-rays. Details of the BL45XU are described elsewhere [20,21]. The 2D-SAXS patterns were recorded with the Hamamatsu image intensifier equipped with a cooled CCD [21,22] and λ was tuned to 0.1015 nm. The 1D-SAXS profiles were converted from the 2D-SAXS patterns by sector averaging with a specified value of the azimuthal angle (μ) with allowances of $\pm 5°$. As shown in Fig. 2, μ is defined as the angle from the meridian.

2.3. H_v-SALS

The light source was a 5-mW He–Ne laser ($\lambda = 632.8$ nm). The scattering patterns impinged on a screen and were captured by a digital camera (Fuji HC-300i). The samples used for measurements were prepared by the following procedure. Solution cast samples were subjected to flow to align micro-LAM structures by applying a planar extensional flow at about 150 °C (well above the T_m of PE) for 2 h [9]. Then the samples were sandwiched between two 1-in. diameter glass disks. The thicknesses of the samples were then adjusted to 80–120 μm at 180 °C. After pre-heating at 180 °C for 30 min., the samples were quickly transferred to the heater block which was kept at a given T_c (93–101 °C) until the time evolution of the scattering intensity was saturated. An average spherulite size, R_s, was calculated from the peak position, q_m, in the H_v-SALS pattern using the following equation [23,24].

$$R_s = 4.09/q_m \quad (1)$$

Here $q_m[= (4\pi/\lambda)\sin(\theta_m/2)]$ is the magnitude of the scattering vector with θ_m being the scattering angle at the peak position in the four-leaf clover patterns.

2.4. DSC measurements

DSC measurements were carried out on SII SSC 5200 differential scanning calorimeter. The measured enthalpy of fusion (ΔH_f) was converted to the degree of crystallinity ($\Delta H_f/(0.48\Delta H_f^*)$) per PE unit (Table 1), with respect to the enthalpy of fusion for the perfect PE crystal ($\Delta H_f^* = 290$ J/g) [16].

Table 1
Enthalpy of fusion (ΔH_f) and crystallinity (%) for the samples isothermally crystallized at 93 and 95 °C

T_c (°C)	ΔH_f (J/g)	Crystallinity (%) (per PE unit)
93.0	15.1	10.8
95.0	22.1	15.9

3. Results and discussion

3.1. Outline of results

To outline results, schematic drawings of the sample preparation and the experimental procedures are presented on a phase–temperature plot in Fig. 1. As stated in Section 1, it is a key of the present study to confirm the anticipated alignment of the micro-LAM structures at the melt state in prior to crystallization. One of the most powerful experimental procedures for this identification is a 2D-SAXS technique. However, the contrast for X-ray is miserably low due to similar values of the electron density for PE and aPP moieties in melts. As a matter of fact, the SAXS intensity was quite weak in the melt. Once the PE moiety crystallizes, however, the contrast between crystalline PE phase and surrounding amorphous (PE + aPP) phase becomes high enough so that we can confirm the alignment of the micro-LAM by the 2D-SAXS measurement at room temperature (Figs. 2 and 3). Visual observation was also available for the quenched sample under the transmission electron microscope (TEM), which is presented in Fig. 4.

Nevertheless, we still needed to eliminate an unfavorable possibility of these results (observed alignment of the micro-LAM below T_m of PE), which might be undergone via crystallization-induced microphase separation. Thus, we have to show direct evidence of the existence of the micro-LAM structures at elevated temperature above T_m of PE. As stated above, it is not available by the SAXS technique. For such a case, structural analyses are generally performed by a small-angle neutron scattering (SANS) technique. In the current study, a deuterated sample was prepared where the PE moiety was perdeuterated. Although the total molecular weight and the composition should be matched with those of the main sample (the non-deuterated DEP113) for rigorous comparison, such a deuterated sample was not available. Instead, we utilized a deuterated sample with similar composition but different (lower) molecular weight (about 60% of the main sample). As a consequence, clear evidence of existence of the micro-LAM structure in the melt was obtained by the SANS measurements (Fig. 5). Since the segregation power is much stronger for the higher molecular weight block copolymer, it is reasonably concluded from

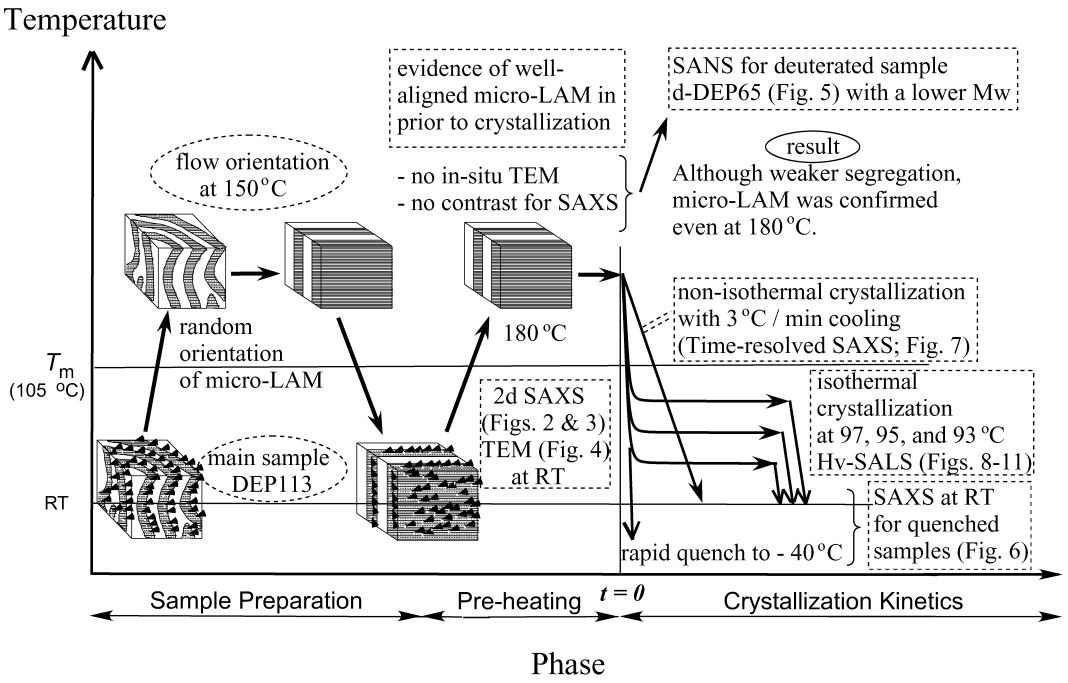

Fig. 1. Schematic drawings for outline of the sample preparation and the experimental procedures.

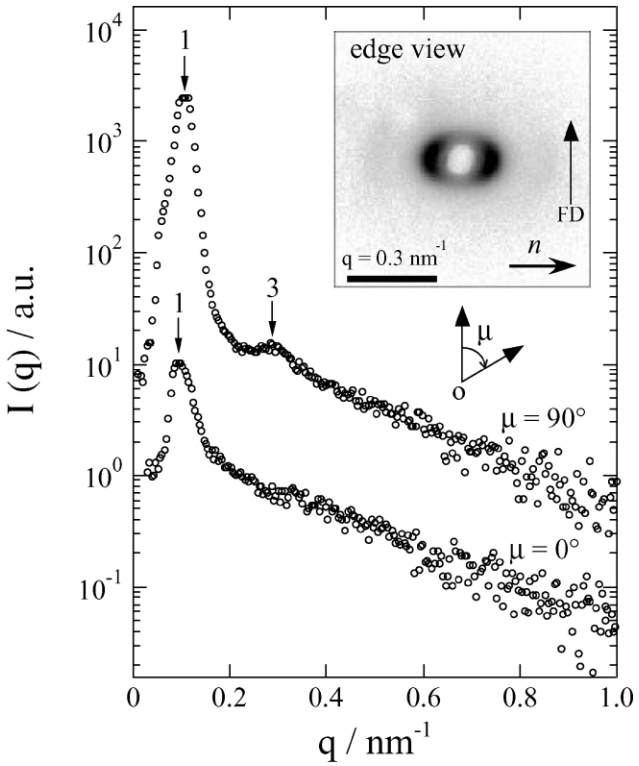

Fig. 2. 1D-SAXS profiles for the edge view of the flow-aligned sample. The edge view was measured by sending incident X-rays from the direction perpendicular to the film normal. The 1D-SAXS profiles were converted from the 2D-SAXS pattern (inset; gray scale for the logarithmic intensity) by sector averaging with $\mu = 0 \pm 5°$ and $90 \pm 5°$. Here, μ denotes an azimuthal angle with respect to the meridian of the 2D-SAXS pattern that is parallel to the flow direction.

the SANS results that the main sample (DEP113) forms micro-LAM structures in the melt.

With the clear evidence of the well-aligned micro-LAM structures at the melt state, first we analyzed crystalline structures formed in the sample being rapidly quenched to −40 °C or in the samples quenched to room temperature from 93 to 97 °C after isothermal crystallization. For this purpose, static 1D-SAXS measurements were conducted at room temperature (Fig. 6). Finally, both non-isothermal and isothermal crystallization processes were studied by using the well-aligned micro-LAM structures. While the latter was followed by H_v-SALS for the study of spherulite growth (Figs. 8–11), the non-isothermal crystallization experiment was conducted (Fig. 7) in order to explain the

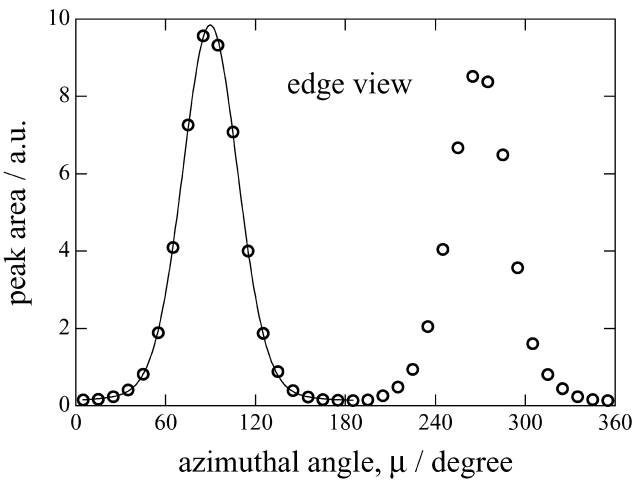

Fig. 3. Distribution of the peak area ($\int_{q_1}^{q_2} I(q)q^2\,dq$ in the range of $q_1 \le q \le q_2$ around the first-order peak) as a function of the azimuthal angle, μ.

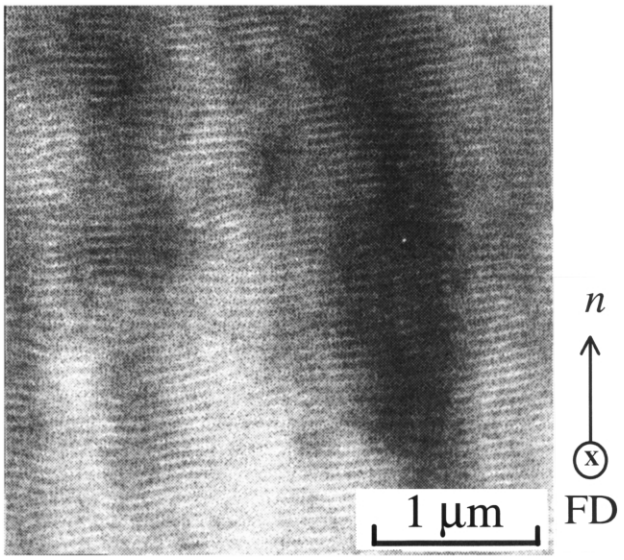

Fig. 4. Bright-field TEM micrograph for a thin section from the rapidly quenched DEP113 sample, which was subjected to extensional flow at about 150 °C for 2 h in advance, without being stained. Due to the diffraction contrast, the PE microdomains that contain crystallites appear dark. Here, FD and n denote the flow direction and the direction normal to the sample film, respectively.

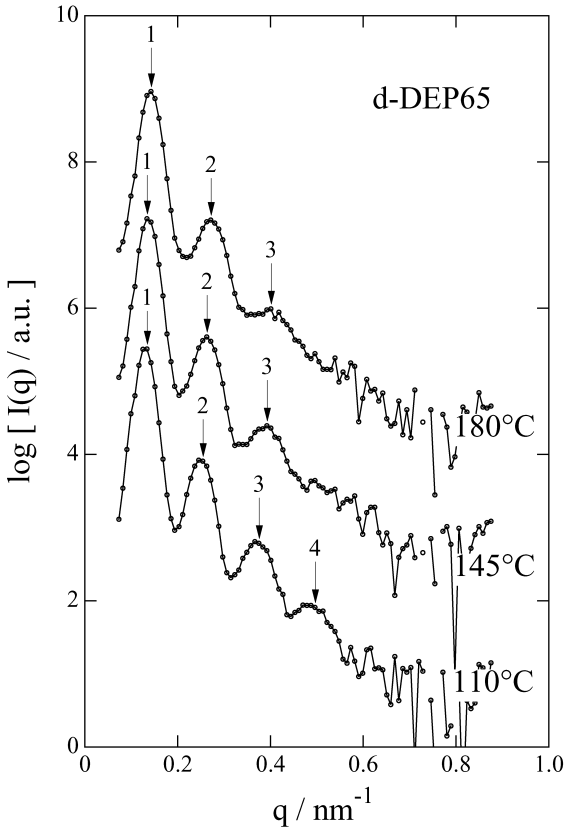

Fig. 5. SANS profiles [log $I(q)$ vs. q] measured at 110, 145, and 180 °C for a deuterated sample (d-DEP65), of which PE moiety is perdeuterated, having smaller molecular weight as compared to that of DEP113, i.e. $M_w = 64.8$ kg/mol and $M_w/M_n = 1.07$. Here, q denotes the magnitude of the scattering vector.

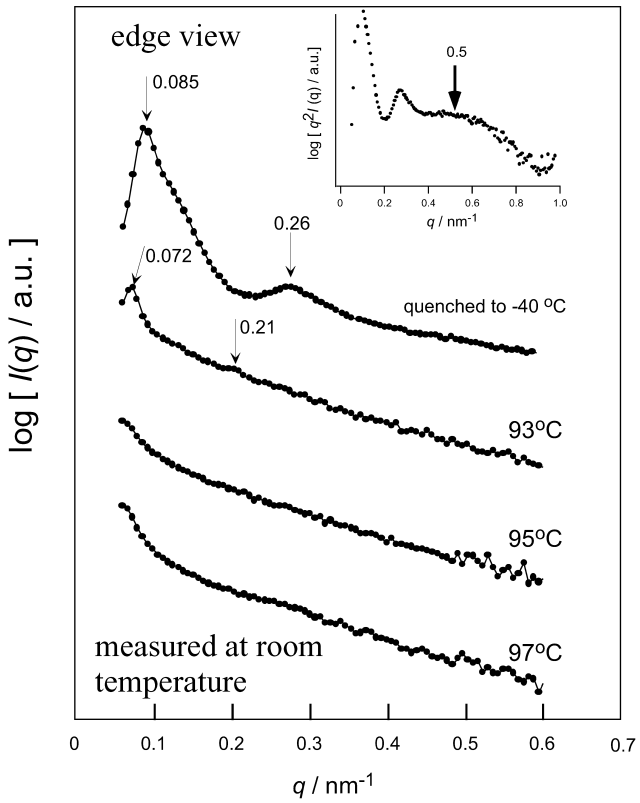

Fig. 6. SAXS profiles for a sample quenched rapidly to −40 °C from the melt and samples quenched from the isothermal crystallization at 93, 95, and 97 °C, where all profiles were measured at room temperature. The logarithm of the Lorentz-corrected scattering intensity, $\log[q^2 I(q)]$, is plotted as a function of q for the sample rapidly quenched to −40 °C.

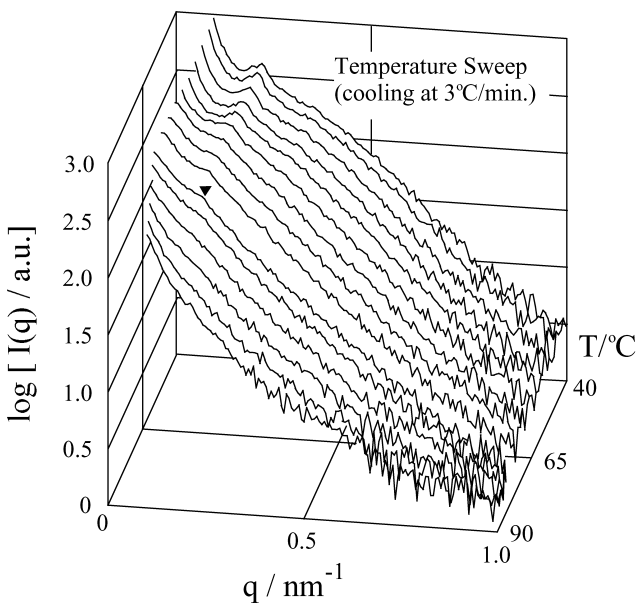

Fig. 7. Temporal change in the SAXS profile upon non-isothermal crystallization by cooling a sample from the melt state at 3 °C/min. A filled triangle is labeled on the profile obtained at 86 °C in order to indicate the third-order diffraction peak at $q = 0.224$ nm^{-1}, which is attributed to the micro-LAM structures.

conservation of the micro-LAM structure during the isothermal crystallization at 93 °C (Fig. 6).

3.2. 2D-SAXS results

A 2D-SAXS pattern from the edge view of the flow-oriented sample is presented in Fig. 2 (inset; gray scale for the logarithmic intensity), where q denotes the magnitude of the scattering vector. Note here that the edge view was measured by sending incident X-rays from the direction perpendicular to both the film normal and the flow direction. Here, μ denotes the azimuthal angle with respect to the meridian of the 2D-SAXS pattern, which was parallel to the flow direction. The 1D-SAXS profiles were converted from the 2D-SAXS pattern by sector averaging with $\mu = 0 \pm 5°$ and $90 \pm 5°$. In the profile for $\mu = 90°$, first- and third-order diffraction peaks are clearly seen at $q = 0.10$, and $0.29\ \mathrm{nm}^{-1}$, respectively, which can be ascribed to the micro-LAM structure that alternate in one-dimension. Here, the second-order lattice peak was not observed because the particle scattering function was almost zero at the q value where the second-order diffraction peak would have appeared. This phenomenon occurs in the case of a nearly identical thickness of each micro-LAM [25], such as the present DEP113 sample. On the other hand, only a relatively weak first-order peak can be observed in the profile for $\mu = 0°$. These facts indicate a preferential orientation of the micro-LAM structures with respect to the film surface, i.e. the interface between micro-LAM structures is almost parallel to the film surface and to the planar extensional flow.

For a more quantitative discussion of the preferential orientation of the micro-LAM structure, we evaluated the second-order orientation factor, F_2 for the orientation of the micro-LAM structure. The distribution of the peak area ($\int_{q_1}^{q_2} I(q)q^2\,\mathrm{d}q$ in the range of $q_1 \le q \le q_2$ around the first-order peak) as a function of the azimuthal angle μ was extracted from the 2D-SAXS pattern and is shown in Fig. 3. According to the previously reported procedure [26], we evaluated a second-order orientation factor, F_2, as big as 0.70 for this particular case. Thus, we could obtain highly aligned micro-LAM structures in the flow-oriented sample film, which enabled us to examine whether such structures can be sustained and co-exist with evolving spherulite and to investigate effects of dimensionality on crystallites growth in the confined space.

3.3. TEM result

Visual evidence of the existence of the well-aligned micro-LAM structures at 150 °C was obtained by conducting TEM on the rapidly quenched DEP113 sample, which was in prior subjected to extensional flow at about 150 °C for 2 h in advance. Fig. 4 displays a bright-field TEM micrograph for a thin section from the quenched DEP113 sample without being stained. Due to the diffraction contrast, the PE microdomains that contain crystallites appear dark. In Fig. 4, well-aligned micro-LAM structures are seen. Here, FD and n denote the flow direction and the direction normal to the sample film, respectively. Therefore, the TEM result definitely confirms that the micro-LAM structures preferentially aligned parallel to the planar extensional flow [9,15].

3.4. SANS results

The sample used (d-DEP65), of which PE moiety is perdeuterated, has a smaller molecular weight as compared to that of DEP113, i.e. $M_w = 64.8$ kg/mol and $M_w/M_n = 1.07$, and the volume fraction of the PE blocks in the melt state was 0.52. The measurement was conducted at the Cold Neutron Research Facility of the National Institute of Standards and Technology in Gaithersburg, Maryland. Refer to the previous paper for details of the measurement [9]. The obtained SANS profiles [log $I(q)$ vs. q] at 110, 145, and 180 °C are presented in Fig. 5. Diffraction peaks were clearly observed at relative q positions of 1: 2: 3, indicating the existence of micro-LAM structures in the range from 110 to 180 °C. Considering the higher molecular weight of the DEP113, the DEP113 sample is well in the strong-segregation regime and therefore the SANS result for d-DEP65 suggests that the DEP113 sample undergoes microphase separation to form micro-LAM structures in the melt.

It is worth estimating the order–disorder transition temperature (T_{ODT}) of the DEP113 sample for the sake of comparison of quench depth for microphase separation with that for crystallization. Using the temperature-dependent solubility parameter values reported by Graessley and coworkers [27,28], the temperature-dependent χ values can be estimated as

$$\chi = -0.0855 + 51.5/T \tag{2}$$

for the PE/aPP segmental pair (taking the segment containing four carbon atoms for PE and that containing six carbon atoms for aPP). The number of segments, N, is therefore calculated to be 1652. Assuming $\chi N = 10.5$ at T_{ODT} for simplicity, we estimated $T_{ODT} = 290$ °C. Thus, the estimated T_{ODT} is far above the crystallization temperatures (93–101 °C) examined in the present study. We further estimated the degree of segregation at 95 °C, which was found $\chi N = 90$, indicating that the DEP113 sample is in the strong-segregation regime.

3.5. Static 1D-SAXS results

SAXS profiles (edge view) are shown in Fig. 6 for a sample quenched rapidly to −40 °C from the melt and samples quenched from the isothermal crystallization at 93, 95, and 97 °C, where all profiles were measured at room temperature. The profile for the sample rapidly quenched to −40 °C exhibits clear first- and third-order diffraction peaks

at $q = 0.085$ and 0.26 nm^{-1}, respectively. Note here that we carefully conducted optical collimation of the SAXS camera so as to measure a lower q region as much as possible. Otherwise, the first-order peak position is so small that we cannot detect it with a normal collimation condition. Similarly, the '93 °C' profile shows first- and third-order diffraction peaks at $q = 0.072$ and 0.21 nm^{-1}, respectively. Therefore, for those samples it is considered that the crystallization proceeded without overwhelming the pre-existing micro-LAM structures. As a matter of fact, it is found that the cryst-LAM co-exists with the micro-LAM, because the broad peak being ascribed to the long period of the cryst-LAM is present around $q = 0.5$ nm^{-1}, as shown in the inset, where the logarithm of the Lorentz-corrected scattering intensity, $\log[q^2 I(q)]$, is plotted as a function of q for the sample rapidly quenched to −40 °C. On the other hand, the '95 °C' and '97 °C' profiles exhibit no first-order diffraction peaks from the micro-LAM structures. Instead, there is an upturn in the scattering intensity in the low q region, implying the presence of ill-ordered microdomain structures with larger size. Although the data are not presented here, when crystallized at 91 or 87 °C, there were clear first- and third-order diffraction peaks from the micro-LAM structure. On the other hand, when crystallized at 99 and 101 °C, there were no such diffraction peaks. We also carried out the isothermal crystallization at 95 °C to see whether the micro-LAM structure was preserved or not. However, the result was stochastic. In most cases we could not see any diffraction peak from the residual micro-LAM structure, while in a few cases the first-order diffraction was observed around 0.07 nm^{-1}. This stochastic result was due to difficulty in controlling sample temperature when cooled from the melt. Thus, 95 °C seems to be close to the crossover temperature from a preservation regime of the micro-LAM (at lower temperatures) to a spherulite growth regime (at higher temperatures).

Let us discuss the position of the first-order peak at $q = 0.072$ nm^{-1} for the profile for $T_c = 93$ °C in Fig. 6. As compared to the result obtained for the sample quenched from 150 °C, which shows the peak around $q = 0.10$ nm^{-1} in Fig. 2, the micro-LAM spacing is found to be increased. Simple temperature dependence of the micro-LAM spacing (d) [29], which is $d \sim T^{-1/3}$ (T: absolute temperature), can hardly account for the increase at 93 °C as compared to the case at 150 °C. It seems that crystallization of the PE moiety within its micro-LAM space may enlarge the domain spacing, suggesting a precursory stage of rupture of the micro-LAM structures.

3.6. Time-resolved 1D-SAXS results (non-isothermal crystallization)

Fig. 7 displays the temporal change in the SAXS profile upon crystallization by steadily cooling the sample from the melt state at 3 °C/min (non-isothermal crystallization). The third-order diffraction peak attributed to the well-ordered micro-LAM structure emerged below ca. 86.0 °C, as marked by a filled triangle at $q = 0.224$ nm^{-1} around 86 °C, indicating that the pre-existing micro-LAM structure remained even at this cooling rate (3 °C/min). Due to a crucially low contrast for X-rays between the PE and aPP moieties in the melt, no diffraction peak, if any, can be identified. During the cooling process, crystallites form in the PE micro-LAM space, which provides sufficient X-ray contrast against the aPP moiety. As a matter of fact, a broad shoulder appeared around $q = 0.5$ nm^{-1} in the Lorentz-corrected intensity plot in prior to the evolution of the peak at $q = 0.224$ nm^{-1} around 86 °C. This clearly suggests that the crystallization in the PE microdomains improved the contrast for X-rays, which in turn highlighted pre-existing micro-LAM structures. Since the peak at $q = 0.224$ nm^{-1} corresponds to the third-order diffraction maximum, the first-order peak position is expected to be at $q = 0.075 \times$ nm^{-1}. This indicates that the domain spacing is larger than that for the quenched sample, as well as the case for $T_c =$ 93 °C discussed above in Fig. 6. Note here that the deficiency of lower q resolution to cover the first-order peak around 0.08 nm^{-1} in this particular case is due to a normal collimation condition where the minimum detectable q value is 0.08 nm^{-1}.

At a glance, the micro-LAM in the melt might be conserved due to the rapid quench. However, even at a slower quench with 3 °C/min cooling, the conservation was confirmed to some extent (Fig. 7). This result clearly indicates that the cooling rate is not a key factor. As compared to the structure in the sample rapidly quenched to −40 °C, the dominant size of the crystalline microdomain structures is found to be slightly larger because the third-order peak appeared in a lower q range ($q = 0.224$ nm^{-1}). Rather, the position of the third-order peak is close to that for the sample isothermally crystallized at 93 °C. Thus, the crystalline microdomain structure is considered to form around 93 °C, although the peak became clearly identified around 86 °C. Slight difference in the temperature may be due to non-isothermal process. Moreover, the position of the third-order peak did not appreciably change during the non-isothermal crystallization process. Therefore, in the successive non-isothermal process where the sample temperature continuously decreased, the crystalline microdomain structure was conserved. Moreover, it is also suggested that isothermal crystallization at lower temperature may lead to a smaller size of the conserved microdomain structure. These facts indicate that the crystallization rate is a key factor. When the crystallization is slower at higher crystallization temperature (of course below the equilibrium melting temperature, T_m^0, of PE moiety), the micro-LAM structure is ruptured, as suggested by the results of SAXS in Fig. 6 for the isothermal crystallization at 95 or 97 °C. Moreover, even for the isothermal crystallization at 93 °C where the micro-LAM was conserved to some extent, the crystalline microdomain structures seem to expand due to crystallization. Refer to the discussion given in Section 3.8.

3.7. H_v-SALS results (isothermal crystallization)

We discuss on the spherulite formation based on the H_v-SALS results. When the sample was cooled at 10 °C/min from the melt, no H_v scattering was observed. Since a four-leaf clover H_v-SALS pattern is evidence of spherulite formation, its absence means this cooling rate was too fast for the sample to generate a spherulite. Generally speaking, the polyethylene homopolymer (homo-PE) can yield a well-developed spherulite even at a cooling rate greater than 10 °C/min [30]. Therefore, our experimental result is associated with the nature of the semi-crystalline block copolymer. That is, the amorphous aPP block chain bound to the crystalline PE block obstructs the crystallization of the PE block chains. Moreover, we found that when the same sample was cooled slowly by taking a few days, spherulites developed and there was no trace of the micro-LAM structure [17]. Therefore, we consider that the crystallization rate is crucial to determine final morphology for the DEP113 sample, and we decided to examine carefully the relationship between crystallization rate (i.e. temperature of the isothermal crystallization) and the final morphology.

To study spherulite formation even in the strong-segregation regime, the pre-existing micro-LAM structure in the DEP113 sample was oriented in advance by imposing an extensional flow at about 150 °C for 2 h. Fig. 8 compares the H_v-SALS results obtained for the isothermal crystallization at 93, 95, 97, and 99 °C. No appreciable four-leaf clover pattern is observed at 93 °C. On the other hand, a four-leaf clover pattern was seen at the other temperatures. The 1D H_v-SALS profile for $\mu = 45°$ was obtained by sector averaging the 2D H_v-SALS pattern with $\mu = 45 \pm 5°$ and is shown in Fig. 9. With increasing T_c, the peak position shifts to lower q and its intensity increases. Recall here that the peak position is related to the size of spherulite. To evaluate R_s using Eq. (1), the peak position q_m needs to be determined. However, the determination was not straightforward due to scatter in the data points around a peak. Furthermore, the contribution of the background was not negligible, as can be seen in the profile for $T_c = 93$ °C. For the sake only of an accurate determination of the peak position, we conducted curve fitting using a phenomenological mathematical formulation composed of the Gaussian function with a monotonic intensity decay with q (actually the Lorentzian function with a maximum at $q = 0$ was utilized). Thus it is anticipated that the estimated R_s increased with an increase of T_c (this plot is actually shown later in Fig. 11(b)).

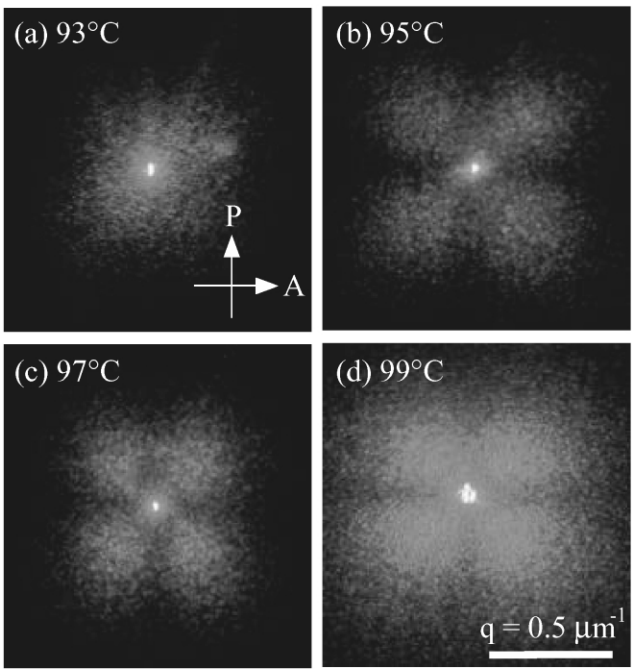

Fig. 8. H_v-SALS patterns obtained for the isothermal crystallization at 93, 95, 97, and 99 °C.

Time evolution in the 1D H_v-SALS profile for $\mu = 45°$ is presented in Fig. 10(a) and (b) during the isothermal crystallization at 97.0 and 99.0 °C, respectively, upon quenching after pre-heating of the sample at 180 °C for 30 min. Fig. 11 shows the time course of R_s for $T_c = 97.0$ and 99.0 °C. At 99.0 °C, R_s increased in a similar manner to that at 97.0 °C, but the linear growth rate was about 1.5 times slower than in the case for crystallization at 97.0 °C.

It has been shown by the SAXS and SALS studies that spherulites can grow even if the crystallization is initiated within the spatially confining micro-LAM space when the crystallization temperature is above 95 °C. However, the

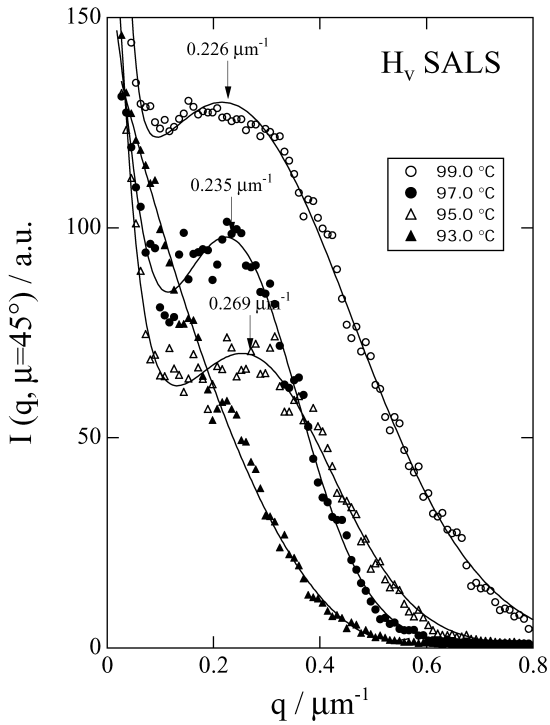

Fig. 9. 1D H_v-SALS profiles for samples isothermally crystallized at 93, 95, 97, and 99 °C. Note that the 1D profile was converted from the 2D pattern by sector averaging with $\mu = 45 \pm 5°$.

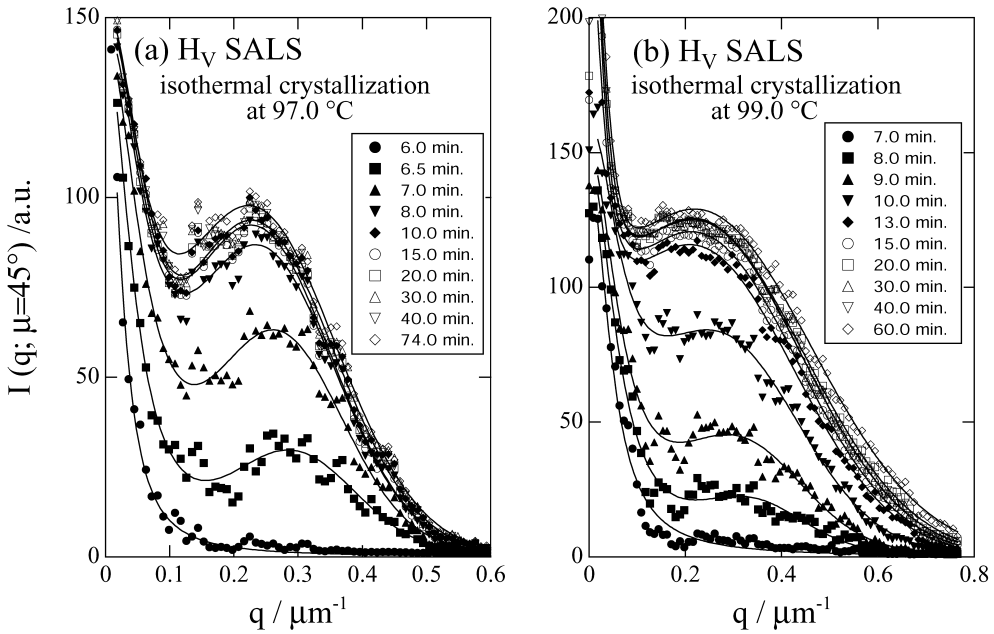

Fig. 10. Time evolution in the 1D H_v-SALS profile during the isothermal crystallization at (a) 97.0 and (b) 99.0 °C, upon quenching after pre-heating the sample at 180 °C for 30 min.

crystallization was much retarded as compared to that below 95 °C and to the general case of homo-PE [16]. It is of great interest to examine whether the spherulite and micro-LAM structures co-exist or not. The SAXS results indicate that the micro-LAM structure can be preserved when the sample is cooled at 3 °C/min and also isothermally crystallized at T_c below 95 °C. However, in this case the SALS results indicated that no spherulites formed. On the contrary, the micro-LAM structure cannot be retained when crystallized at T_c above 95 °C where formation of the spherulite was confirmed. These results imply that there was no co-existence of spherulites and micro-LAM structures, and that 95 °C is close to the crossover temperature from a regime preserving the micro-LAM (at lower T_c) to a spherulite growth regime (at higher T_c).

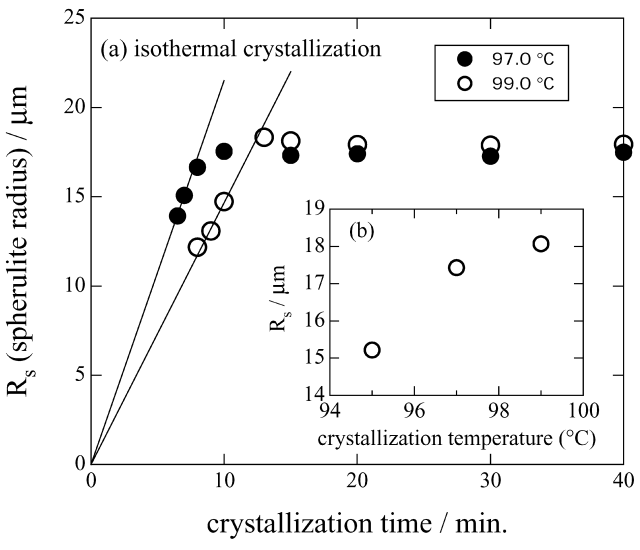

Fig. 11. Time course of the radius of spherulite, R_s, for 97.0 and 99.0 °C.

3.8. Characteristic crystallization of the semi-crystallizable block copolymers

The crystallization was found to be much retarded for DEP113 as compared to the case of homo-PE [16]. A rate-determining process in the crystallites growth is diffusion of the crystallizable block chain that is attached to a growth face of crystallites [31]. Since it is necessary that the chemical junctions of the block copolymer are localized in the interfacial region in the strong-segregation regime, the junctions are not very mobile and the crystallizability are lowered. Moreover, the presence of the non-crystallizable aPP block chains in the proximity of the growth face of crystallite obstructs its growth. Similar arguments have been made by several authors. In particular, Shiomi et al. [32] have evaluated the tremendously high activation energy for the crystallization of semi-crystalline block copolymers in which the counterpart of non-crystallizable block chain is in the glassy state. Our finding of a slow-growth rate of spherulite can be ascribed to such factors.

Generally speaking, the thermodynamic driving force for crystallization is larger when the quench is deeper. The fact that spherulites formed for $T_c = 95–99$ °C (Fig. 8(b)–(d)) while not for $T_c = 101$ °C is in accord with this concept. Note here that T_m is 105 °C for the DEP113 sample. Therefore, it might be concluded that the lower crystallization temperature results in easier formation of spherulites. However, for much deeper quenches there were no spherulites (Fig. 8(a)). Within the experimentally examined temperature range (86–101 °C) it was expected that the

DEP113 sample was in the strong-segregation regime so that the degree of the spatial constraint due to the microphase separation hardly changes over this range of crystallization temperature. Therefore, it is important to take into account the following *auto-decelerating effect* of nuclei in a confining microdomain space. The formation of a nucleus may suppress the mobility of crystallizable chains in a confining microdomain space. At a much lower crystallization temperature, numerous nuclei form and are distributed in the confined space. Fine-grained distribution of the nuclei can pin crystallizable chains down in the amorphous state and hence the nuclei cannot grow further into spherulites. Note that impingement of spherulites is not the issue. Since the number of nuclei is smaller at $T_c = 95-97\,^{\circ}C$, the nuclei can grow finally into spherulites by breakout from the confined space, though the crystallization dynamics are slow. As a matter of fact, crystallinity was found to be lower for the lower crystallization temperature by the DSC results (Table 1).

4. Conclusions

The characteristics of crystallization in a semi-crystalline block copolymer were experimentally examined using SAXS and H_v-SALS techniques. First of all, crystallization was found to be much suppressed as compared to that of homo-PE [9]. At a higher crystallization temperature ($T_c = 101\,^{\circ}C$), no spherulites formed. On the contrary, the spherulite growth was found to rupture the micro-LAM structures at an intermediate crystallization temperature ($95 < T_c < 101\,^{\circ}C$). Thus, the spherulites can grow even if crystallization is initiated in the spatially confining micro-LAM structures. However, it was further found that the micro-LAM structures did not co-exist with spherulites. At even lower crystallization temperatures ($T_c < 95\,^{\circ}C$), the micro-LAM structure was retained whereas no spherulites formed. This re-entrant type of suppression of spherulite formation may be accounted for by an auto-decelerating effect of nuclei in a confining microdomain space.

Overall, we clearly showed experimental results that the micro-LAM structures and spherulites did not co-exist when the material crystallizes from the pre-existing micro-LAM structures. Moreover, spherulites can grow from the pre-existing micro-LAM structures even in the strong-segregation regime. Here, it is important to correlate the formation of spherulites to stem orientation. Recently, work has been conducted by several groups using well-aligned microdomain structures to reveal the relationship between microdomain structures and crystallites, which include careful studies of stem orientation in the spatially confined microdomain space [33–35]. In our previous publication [36], however, a completely different result for the stem orientation was reported; namely, the *b* axis of the PE crystallites was always perpendicular to the normal of the micro-LAM, while the *a* and *c* axes rotated with respect to the *b* axis. This implies that the crystalline fibrils twist in the confined micro-LAM space when the micro-LAM is preserved. On the contrary, we deduced branching of the crystalline fibrils when the micro-LAM was ruptured and the spherulites formed. Therefore, the twisting can be considered as a precursory step for the fibril branching, and whether the fibril branches or not may account for the whole story of our T_c-dependent results, as discussed above.

Acknowledgements

This work was supported in part by a research grant from Kinki Invention Center (granted to S.S.). The SAXS experiments were performed in the Photon Factory of the Research Organization for High Energy Accelerator with the approval number 99G241, and at SPring-8 (2000B0228-NOL).

References

[1] Sakurai S. Trends Polym Sci 1995;3:90.
[2] Rangarajan P, Register RA, Fetters LJ. Macromolecules 1993;26:4640.
[3] Cohen RE, Cheng PL, Douzinas K, Kofinas P, Berney CV. Macromolecules 1990;23:324.
[4] Seguela R, Prud'homme J. Polymer 1989;30:1446.
[5] Nojima S, Kato K, Yamamoto S, Ashida T. Macromolecules 1992;25:2237.
[6] Ryan AJ, Hamley IW, Bras W, Bates FS. Macromolecules 1995;28:3860.
[7] Douzinas KC, Cohen RE. Macromolecules 1992;25:5030.
[8] Rangarajan P, Register RA, Adamson DH, Fetters LJ, Bras W, Naylor S, Ryan AJ. Macromolecules 1995;28:1422.
[9] Sakurai K, Lohse DJ, Schulz DN, Sissano J, Lin MY, Agamalyan M, Linand J, MacKnight WJ. Polymer 1996;37:4443.
[10] Inaba N, Yamada T, Suzuki S, Hashimoto T. Macromolecules 1988;21:407.
[11] Terada Y, Ikehara T, Nishi T. Polym J 2000;32:900–3.
[12] Rangarajan P, Register RA, Fetters LJ, Bras W, Naylor S, Ryan AJ. Macromolecules 1995;28:4932.
[13] Kofinas P, Cohen RE. Macromolecules 1995;28:336.
[14] Hashimoto T, Koizumi S, Hasegawa H. Macromolecules 1994;27:1562.
[15] Hong S, Bushelman AA, MacKnight WJ, Gido SP, Lohse DJ, Fetters LJ. Polymer 2001;42:5909.
[16] Alamo RG, Mandelkern L. Macromolecules 1991;24:6480.
[17] Sakurai K, Lohse DJ, Schulz DN, Sissano J, MacKnight WJ. Macromolecules 1994;27:4941.
[18] Amemiya Y, Wakabayashi K, Hamanaka T, Wakabayashi T, Hashizume H. Nucl Instrum Method 1983;208:471–7.
[19] Amemiya Y, Ito K, Yagi N, Asano Y, Wakabayashi K, Ueki T, Endo T. Rev Sci Instrum 1995;66:2290.
[20] Fujisawa T. J Jpn Soc Synchrotron Radiat Res 1999;12:194.
[21] Fujisawa T, Inoue K, Oka T, Iwamoto H, Uruga T, Kumasaka T, Inoko Y, Yagi N, Yamamoto M, Ueki T. J Appl Crystallogr 2000;33:797–800.
[22] Fujisawa T, Inoko Y, Yagi N. J Synchrotron Radiat 1999;6:1106.
[23] Stein RS, Rhodes MB. J Appl Phys 1960;31:1873.
[24] Stein RS, Wilson PR. J Appl Phys 1962;33:1914.

[25] Sakurai S, Okamoto S, Kawamura T, Hashimoto T. J Appl Crystallogr 1991;24:679–84.
[26] Sakurai S, Aida S, Okamoto S, Ono T, Imaizumi K, Nomura S. Macromolecules 2001;34:3672.
[27] Graessley WW, Krishnamoorti R, Balsara NP, Butera RJ, Fetters LJ, Lohse DJ, Schulz DN, Sissano JA. Macromolecules 1994;27:3896.
[28] Graessley WW, Krishnamoorti R, Reichart GC, Balsara NP, Fetters LJ, Lohse DJ. Macromolecules 1995;28:1260.
[29] Hashimoto T, Shibayama M, Kawai H. Macromolecules 1980;13:1237.
[30] Maxfield J, Mandelkern L. Macromolecules 1977;10:1141.
[31] Lauritzen JI, Hoffman JD. J Res N B S 1960;64A:73.
[32] Shiomi T, Tsukada H, Takeshita H, Takenaka K, Tezuka Y. Polymer 2001;42:4997.
[33] Park C, De Rosa C, Fetters LJ, Thomas EL. Macromolecules 2000;33:7931.
[34] Zhu L, Cheng SZD, Calhoun BH, Ge Q, Quirk RP, Thomas EL, Hsiao BS, Yeh F, Lotz BJ. Am Chem Soc 2000;122:5957.
[35] Loo Y-L, Register RA, Adamson DH. Macromolecules 2000;33:8361.
[36] Sakurai K, Shinkai S, Ueda M, Sakurai S, Nomura S, MacKnight WJ, Lohse DJ. Macromol Rapid Commun 2000;21:1140.